

CNN-BASED UNSUPERVISED REGISTRATION OF TIME-LAPSE MICROSCOPY IMAGE SEQUENCES

N. A. Anoshina, D. V. Sorokin*

Laboratory of Mathematical Methods of Image Processing, Faculty of Computational Mathematics and Cybernetics,
Lomonosov Moscow State University, Moscow, Russia - (n.anoshina@cs.msu.ru, dsorokin@cs.msu.ru)

Commission II, WG II/8

KEY WORDS: Image Registration, Deep Learning, Convolutional Neural Networks, Live Cell Imaging

ABSTRACT:

Image registration is widely used in live cell microscopy image analysis to compensate for the cell motion. It is a challenging task as the cell is not only moving (which causes rotation and translation), but also changes its form in time making the motion non-rigid. To address this, we propose a CNN-based unsupervised method for non-rigid registration of live cell image sequences. Our network predicts both the deformation field between a pair of images of the sequence and an affine transformation matrix for the cell motion compensation. The method can be used alone or in combination with other approaches. The proposed approach was successfully applied to real live cell microscopy image sequences. We conducted an experimental comparison with existing methods including contour-based, intensity-based and a deep learning based joint denoising and registration method. In addition, we analyzed different deformation regularizers and their impact on the alignment results. In combination with contour-based method we outperformed the existing approaches in average registration accuracy for two metrics on the standard evaluation dataset.

1. INTRODUCTION

The analysis of cell and subnuclear structures motion is very important in live cell microscopy. It is used to better understand biological processes such as DNA replication, DNA repair, nucleoli assembly, or viral defense. The cell movement is the composition of its local movement and the global motion of the nucleus. To compensate for the cell motion and deformation of temporal live cell sequences in biomedical analysis, image registration is used. Since the cell not only moves but also changes its form over time, compensating for its motion is a very challenging task. With the help of image registration, all images of a temporal sequence are aligned with a reference time point, which is usually the first image of the sequence. This way, image registration helps to determine and analyze the local motion of subcellular particles, which is usually the subject of the study.

The previous works on biomedical image registration methods can be divided into two groups: classical and learning-based approaches. Among the classical methods, there are rigid intensity-based approaches: in (Wilson and Theriot, 2006) and (Goobic et al., 2005), authors described correlation-based approaches for rigid registration. In (van de Giessen et al., 2011), an estimated photobleaching model is used to compensate for the linear motion in FLIP sequences. In (Raza et al., 2012), the authors proposed a block-based method for registration of color channels in multi-tag fluorescence microscopy images. In (Ozere et al., 2013), a parametric stabilization method for global motion and intensity variation estimation was presented. Other classical methods do not take the intensity into account: there is a contour-based approach that performs non-rigid registration (Sorokin et al., 2018); authors used a dynamic elasticity model for the forward simulation of nucleus motion and deformation based on the motion of its contours. In (Matula

et al., 2006), the authors proposed using the subcellular structures' positions for deriving a rigid transform between different images. In addition, there are optical flow-based methods that are based on well-founded models of cell motion or other physical principles and have proved their effectiveness in practical applications. In (Kim et al., 2010), the authors extended the Lucas-Kanade optical flow model for deformation field estimation between consecutive frames. Then this work was continued by (Tektonidis et al., 2015) where the authors added a multi-frame extension and improved noise robustness. In (Gao and Rohr, 2019), the authors introduced a global optical flow model for non-rigid cell image registration.

The group of learning-based biomedical image registration methods has proved to be very efficient in terms of fast computational time. Their advantage is learning the motion from the data itself. However, they suffer from the requirement of a large amount of training data. Also, the supervised approaches require expert annotation for the training procedure. Initially, unsupervised deep learning approaches (Balakrishnan et al., 2019) for non-rigid registration and (De Vos et al., 2019) for rigid and non-rigid registration were proposed for use in medical imaging (MRI, CT, or ultrasound) and performed better and faster than traditional iterative optimization methods (Avants et al., 2008, Avants et al., 2009). Then, (Celikay et al., 2022) proposed a deep learning approach for temporal live cell image sequence registration. Here, apart from rigid registration, the authors performed image denoising, which is important for live cell microscopy images since they are very sensitive to the noise level. Also, the authors combined their approach with non-rigid VoxelMorph (Balakrishnan et al., 2019) and outperformed state-of-the-art non-rigid registration methods.

In this work, we propose a CNN-based unsupervised method for non-rigid registration of live cell image sequences. The proposed approach uses a neural network that predicts not only the deformation field, as in (Balakrishnan et al., 2019), but also

* Corresponding author

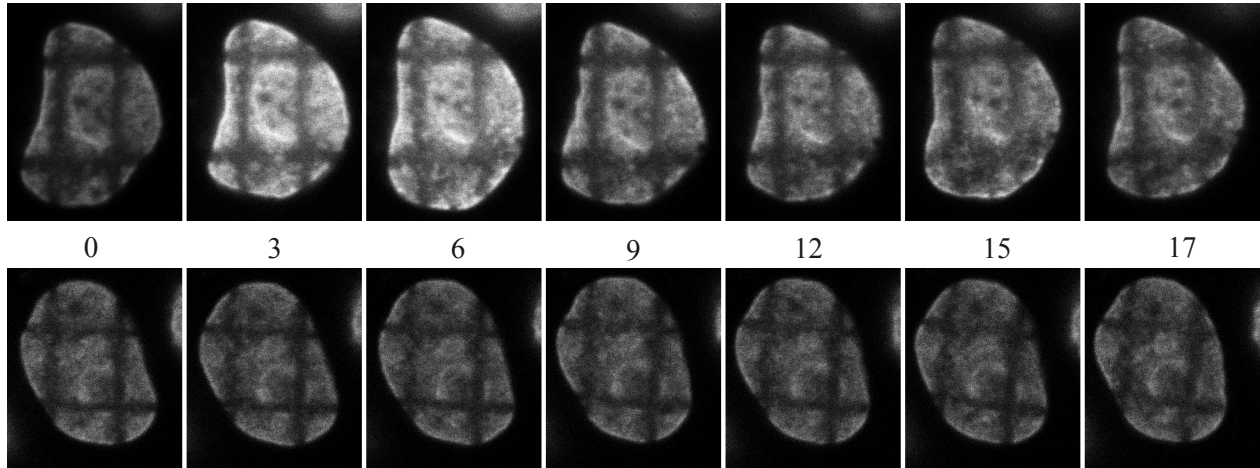


Figure 1. Dataset overview: The horizontal lines present two live cell image sequences. The aim is to align all images in the temporal sequence with a reference time point, which is usually the first image of the sequence, for subsequent analysis. The digits represent timesteps.

an affine transformation matrix inspired by (Jaderberg et al., 2015). Thus, the motion in the temporal live cell image sequences is presented as a combination of affine transformation and deformation fields. The use of the affine transformation block is optional and can be turned off. Unlike (Celikay et al., 2022), the proposed approach learns the affine transformation and the non-rigid deformation field in a single end-to-end model. To cope with data noise, we preprocess the data with denoising filters. Our method was evaluated on a standard cell image registration dataset and proved to be effective in combination with the elasticity-based approach (Sorokin et al., 2018). We outperformed the existing methods on the inner point and line features of the evaluation dataset. We used various deformation field regularizers based on deformation elasticity and flow incompressibility and studied their influence on the registration result.

The paper is organized as follows. In the next section, we introduce our CNN-based unsupervised registration approach. Then, we present the experimental results. Finally, we provide a discussion and conclusion.

2. METHOD

The traditional image registration problem for a given pair of images I_m (called *moving image*) and I_f (called *fixed image*) is formulated as following. Let $I_m(x) : \mathbb{R}^2 \mapsto \mathbb{R}$ and $I_f(x) : \mathbb{R}^2 \mapsto \mathbb{R}$ be the moving and fixed images respectively. Image registration aims to estimate a transformation between the fixed and moving images that consists of affine part A_θ , represented by a matrix, and non-rigid part, represented by a deformation field $\phi : \mathbb{R}^2 \mapsto \mathbb{R}^2$, that maps the coordinates of I_f to the coordinates of I_m :

$$(I_m \circ A_\theta) \circ \phi \approx I_f \quad (1)$$

where $I_m \circ A_\theta$ represents I_m transformed using A_θ , and $(I_m \circ A_\theta) \circ \phi$ represents the result of the transformation warped by the deformation field ϕ . The optimization problem is defined as:

$$\hat{\phi}, \hat{\theta} = \arg \min_{\phi, \theta} \mathcal{L}_R(I_f, I_m \circ A_\theta \circ \phi) + \gamma \mathcal{L}_S^i(\phi) \quad (2)$$

where \mathcal{L}_R is a reconstruction loss measuring the dissimilarity between two images and \mathcal{L}_S^i is a smoothness regularizing constraint for the deformation field (see section 2.3). We chose the value of γ for every regularizing constraint to match the order of reconstruction loss function.

The proposed method takes an image pair as an input and performs affine and non-rigid registration. The output is the warped moving image, the deformation field and the affine transformation matrix. We assume the input images to be single-channel (grayscale).

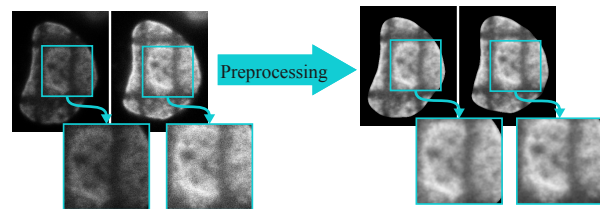


Figure 2. Data preprocessing: a pair of images are normalized, the histograms of the images are matched to the same intensity domain. An image denoising filter and mask multiplication are applied.

2.1 Data Preprocessing

The dataset that is used for CNN training consists of temporal image sequences (Figure 1). On each training iteration, we randomly choose the sequence from the training set and then randomly choose two images. We normalize each image according to its minimum and maximum value. As the cell moves and changes through time, the images can differ in intensity histograms. We perform standard histogram matching to cope with this problem and decrease the registration error. The input of the network is 256×256 , but image sequences in the dataset have different size. Thus, we pad each image to the square shape and then resize it to 256×256 using bilinear interpolation. For augmentation, we use vertical and horizontal

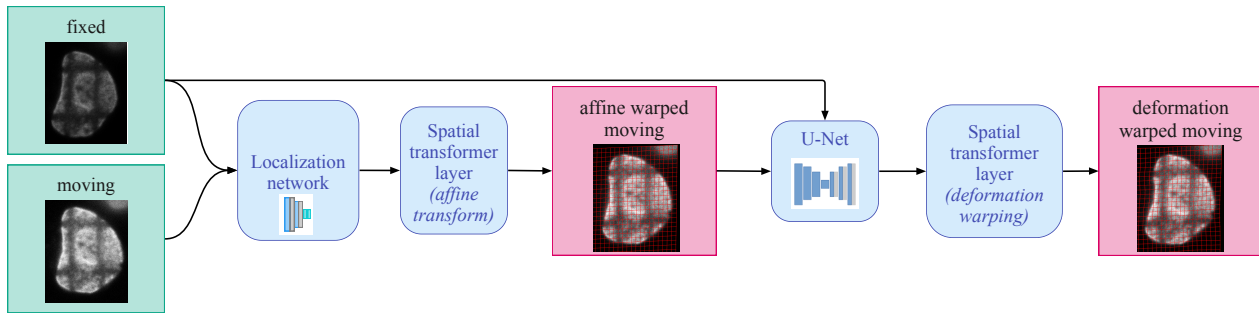


Figure 3. Model architecture: the localization network predicts affine matrix parameters, while a U-Net type convolutional neural network predicts the deformation field. There are two spatial transformer layers to perform warping inside the neural network and compute the loss between the input and warped output.

flips, small translation, rotation and scaling and random brightness changes. We apply the random augmentation to both images. To reduce the noise level, we apply the bilateral filter with $\sigma_{color} = 3.9$ and $\sigma_{space} = 4.4$. There are also cell masks available for the temporal sequences, we multiply each image by the mask to outline cell contours. The result of preprocessing can be seen in Figure 2.

2.2 Model

The architecture (Figure 3) of the proposed convolutional neural network consists of two parts: a localization network for affine transform estimation and a U-Net type network (Ronneberger et al., 2015) for the deformation field estimation. The convolutional blocks of the U-Net type network contain two convolutional layers, each followed by batch normalization and ReLU activation. Then, there is a maxpooling layer with a kernel size of 2. In the decoding path, transposed convolutions are used for upsampling. The localization network consists of two convolutional layers followed by maxpooling layers with ReLU activation and two fully connected layers. The output of the localization network is the affine transformation matrix of size 2×3 .

Initially, the input pair is given to the localization network. Then, inspired by the idea from (Jaderberg et al., 2015), we use a spatial transformer module that explicitly allows the spatial manipulation with data within the network. We apply an affine transform to the moving image as:

$$\begin{pmatrix} x'_i \\ y'_i \end{pmatrix} = A_\theta \begin{pmatrix} x_i \\ y_i \\ 1 \end{pmatrix} = \begin{bmatrix} \theta_{11} & \theta_{12} & \theta_{13} \\ \theta_{21} & \theta_{22} & \theta_{23} \end{bmatrix} \begin{pmatrix} x_i \\ y_i \\ 1 \end{pmatrix} \quad (3)$$

where (x'_i, y'_i) are the coordinates of the transformed regular grid in the moving image, (x_i, y_i) are the initial coordinates in the moving image that define the sample points, and A_θ is the affine transformation matrix. We skip this step if we do not want to use affine registration.

Next, we construct a new pair of input fixed image and affine warped moving image and put it into the convolutional network described earlier. The output is the deformation field ϕ . We use a differentiable spatial transformer layer from (Balakrishnan et al., 2019) to compute $I_m \circ A_\theta \circ \phi$. For each pixel, the corresponding subpixel location is computed as $p' = p + \phi(p)$, using bilinear interpolation.

$$I_m \circ \phi(\mathbf{p}) = \sum_{\mathbf{q} \in \mathcal{Z}(\mathbf{p}')} I_m(\mathbf{q}) \prod_{d \in \{x, y\}} (1 - |\mathbf{p}'_d - \mathbf{q}_d|) \quad (4)$$

where $\mathcal{Z}(\mathbf{p}')$ is the set of pixel neighbours and d iterates over dimensions of image domain Ω .

2.3 Deformation Smoothness Regularizers

To make the deformation field smooth and prevent overfitting, we tested different deformation regularizations:

1. Smoothness constraint (Wahba, 1990):

$$\mathcal{L}_S^1(\phi) = \int_{\Omega} \left(\frac{\partial^2 \phi}{\partial x^2} \right)^2 + \left(\frac{\partial^2 \phi}{\partial y^2} \right)^2 + 2 \left(\frac{\partial^2 \phi}{\partial xy} \right)^2 dx dy \quad (5)$$

2. Elasticity constraint (Gao et al., 2021):

$$\mathcal{L}_S^2(\phi, \mu, \lambda) = \exp \left\{ -\frac{1}{2} \mu s \right\} \cdot \exp \left\{ -\frac{1}{2} (\lambda + \mu) t \right\} \quad (6)$$

where

$$s = \|\mathbf{D}_x u\|^2 + \|\mathbf{D}_y u\|^2 + \|\mathbf{D}_x v\|^2 + \|\mathbf{D}_y v\|^2, \quad (7)$$

$$t = \|\mathbf{D}_x u + \mathbf{D}_y v\|^2$$

μ and λ are Lamé coefficients; $u \in \mathbb{R}^N$ and $v \in \mathbb{R}^N$ are the x - and y -components of ϕ , respectively; \mathbf{D}_x and \mathbf{D}_y are the matrices used to compute the first-order partial derivatives of u and v in the x - and y -directions, respectively; and $\|\cdot\|$ is the l_2 norm.

3. Deformation incompressibility constraint:

Let $I_m(x, y)$ be the density function dependent on time, $I_m = I(x, y, t)$, where the pixel density equals its intensity. Let $I(x, y, 0) = I_m(x, y)$ be the moving image, and $I(x, y, 1) = I_m(x, y) \circ \phi$ be the registered image. Then the total derivative with respect to time is:

$$\frac{dI(x, y, t)}{dt} = \frac{\partial I(x, y, t)}{\partial t} + u(x, y) \frac{\partial I(x, y, t)}{\partial x} + v(x, y) \frac{\partial I(x, y, t)}{\partial y} \quad (8)$$

describes the rate of change of density along the trajectory of image motion. The flow is incompressible when $\frac{dI(x, y, t)}{dt} = 0$. Then, using the condition of flow incompressibility and the continuity equation:

$$\frac{\partial I}{\partial t} + \text{div}(I \cdot \phi) = 0 \iff \frac{dI}{dt} + I \cdot \text{div}(\phi) = 0 \quad (9)$$

Sequence	Inner points					Boundary points					Lines				
	B1	B2	B3	B4	Average	B1	B2	B3	B4	Average	B1	B2	B3	B4	Average
Unregistered	11.3	5.71	8	6.79	7.95	18.15	6.4	9.3	8.13	10.49	22.79	11.37	12.34	11.82	14.58
Contour based	7.92	5.22	2.76	3.04	4.74	3.69	2.02	2.17	2.43	2.58	9.61	7.69	5.23	6.83	7.34
Optical flow based	6.71	4.99	2.35	2.85	4.23	3.36	1.42	1.82	1.86	2.12	N/A				
DenoiseReg	7.46	5.39	2.94	3.18	4.74	4.76	3.07	3.05	2.05	3.23	N/A				
DenoiseReg + VM	6.77	4.74	2.37	3.02	4.23	2.87	1.85	1.77	1.52	2.00	N/A				
Proposed (with \mathcal{L}_S^1)	9.13	5.28	5.04	3.92	5.84	3.39	1.7	1.71	2.61	2.35	11.61	8.11	6.2	7.84	8.44
Proposed (with \mathcal{L}_S^2)	8.23	6.44	3.31	3.34	5.33	3.98	3.29	1.79	1.99	2.76	10.01	8.47	4.62	7.93	7.76
Proposed (with \mathcal{L}_S^3)	10.61	5.26	4.52	3.91	6.06	6.76	3.13	2.52	2.96	3.84	12.2	8.37	6.47	7.36	8.6
Proposed + Contour based (with \mathcal{L}_S^1)	6.79	4.24	2.36	2.72	4.03	3.45	1.88	1.75	2.64	2.43	8.61	7.11	4.24	6.67	6.66
Proposed + Contour based (with \mathcal{L}_S^2)	7.23	4.23	2.43	2.77	4.17	3.51	2.02	1.85	2.55	2.48	8.9	7.13	4.45	6.65	6.78
Proposed + Contour based (with \mathcal{L}_S^3)	7.88	4.73	2.81	3.09	4.63	3.63	1.95	2.02	2.41	2.50	9.32	7.46	4.99	6.89	7.17

Table 1. Experimental results and comparison with other methods: for each sequence, we computed the registration accuracy for boundary, inner, and line features, and averaged it across all features for every image in the sequence.

we obtain the deformation incompressibility condition:

$$\mathcal{L}_S^3(\phi) = \frac{1}{|\Omega|} \sum_{x,y \in \Omega} \|\text{div}(\phi(x,y))\|^2, \quad (10)$$

where $\|\cdot\|$ is the l_2 norm.

We also attempted to use an isotropic total variation regularization term, as introduced in (Sandkühler et al., 2018). However, this term did not perform well with our network.

3. EXPERIMENTAL RESULTS

To evaluate the quality of our proposed approach, we used temporal microscopy image sequences of live cells. The dataset allowed us to compute the registration accuracy of our method and provide a quantitative comparison with other approaches, including the dynamic elasticity contour-based approach (Sorokin et al., 2018), optical flow-based method (Gao and Rohr, 2019), joint registration and denoising method (Celikay et al., 2022) and its composition with VoxelMorph (Balakrishnan et al., 2019). We also compared our approach to its combination with the contour-based method (Sorokin et al., 2018).

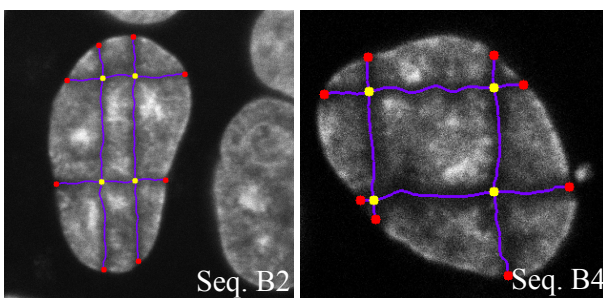


Figure 4. Evaluation dataset: boundary features with red, inner cell features indicated with yellow, and line cell features indicated with magenta. All images in the all sequences in the dataset has annotations for all features.

3.1 Evaluation Dataset

We used a dataset consisting of four live cell microscopy image sequences with laser-induced lines forming a grid on the cell (Sorokin et al., 2014) (see Figure 4). These lines are part of the cell structure, and their motion is caused by the motion of the cell itself. Several features are defined based on

these structures, including boundary- and inner-point features and line features, which enable the evaluation of cell image registration methods by computing the residual error (Sorokin et al., 2018).

3.2 Evaluation Metrics

For each annotated inner and boundary point, we computed the registration error as the Euclidean distance between the current point in the registered image and the first image of the sequence:

$$e_i^k = \|\mathbf{p}_i^k - \mathbf{p}_i^1\| \quad (11)$$

where \mathbf{p}_i^k is the coordinate of the i -th point in the k -th image of the sequence. For the line features, we computed the Fréchet distance between the line feature in the k -th registered image and the first image of the sequence:

$$\mathcal{F}(A_k, A_1) = \inf_{\alpha, \beta} \max_{t \in [0,1]} \{\|A_k(\alpha(t)) - A_1(\beta(t))\|\} \quad (12)$$

where A_k represents the set of current line points in the k -th image of the sequence, α and β are all reparameterizations of $[0, 1]$ of the maximum over all $t \in [0, 1]$. We used bilinear interpolation of the deformation field and performed forward warping for each feature point.

3.3 Results

The registration error e_{mean} averaged over all time points and all line features for Seq. B1–B4 is shown in Table 1. For the methods (Gao and Rohr, 2019, Celikay et al., 2022), we used the metric values reported in the papers only as the source code for these approaches is not publicly available. Thus, we do not provide the values for the line features in Table 1 for these methods, as well as we do not provide visual comparison to these approaches in Fig. 5.

Based on the registration results, it can be concluded that our proposed method, in combination with a contour-based approach, outperforms current state-of-the-art methods in terms of inner-point and line feature registration accuracy. For boundary-point features, our approach improves the results of the contour-based approach. Although, on average, our method performs worse than the DenoiseReg+VM and optical flow-based methods for boundary-point features, it still outperforms these methods on the B2 and B3 sequences. We assume that more robust data denoising is needed to decrease the error of our approach for boundary point features.

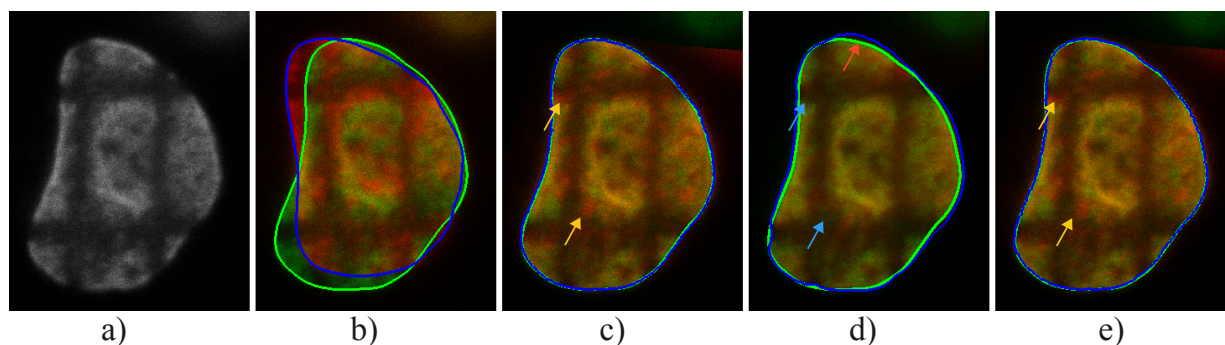


Figure 5. Method comparison for sequence B1: a) First image, b) Unregistered 37-th image, c) Registered by the contour based method 37-th image, d) Registered by the proposed method 37-th image, e) Registered by the combination of the contour based and proposed methods 37-th image. Blue lines represent the current image cell contour overlay, while green lines represent the first image cell contour overlay. Blue arrows indicate places where registration is improved, and orange arrows indicate places where registration is worse compared to other methods. A red arrow shows an error in cell shape prediction.

In the regularization analysis, the deformation smoothness constraint yielded the best results on average across most of the features and sequences in the experiments. Although the elasticity constraint produced better results than the deformation smoothness constraint for some features in sequences B2 and B4 for inner points and lines, the difference was only up to 0.02. The deformation incompressibility constraint performed the worst, except for the boundary points of the B4 sequence. We assume that this outlier behavior is caused by the distinct motion of this cell compared to the others.

4. DISCUSSION

The proposed CNN-based unsupervised registration method was applied to four live cell image sequences. For training, we used random pairs created from two different images of the same sequence. Initially, we trained the model on two sequences (B2 and B4) and additional live cell sequences that did not have feature annotation. We used sequence B1 for validation and tested the model on sequence B3. However, we found that it was difficult for the trained models to generalize well to fully unseen test image sequences. To solve this problem, we added a portion of the sequence into the training process and left the remaining images for testing and validation.

In (Celikay et al., 2022), the authors reported that they randomly split the dataset into 80% training, 10% validation, and 10% evaluation for the B dataset, and used all images for training in another additional dataset. However, evaluating the methods consistently (including previously proposed non-learning based methods) requires computation of the metrics on the entire image sequences, including the training portion of the dataset, which means that the methods are evaluated on data that they have already seen.

In this work, we ended up adopting a similar approach and finally used all images of the sequences to train the model to be consistent with the other methods. We did not consider it an overfitting problem because different cell sequences result in domain shift, where the trained model performs worse for registration. We considered the training process as a self-supervised optimization task, inspired from (Zhu et al., 2021), to improve the generalization accuracy of live cell registration.

5. CONCLUSION

We proposed a CNN-based unsupervised registration method for time-lapse microscopy image sequences, which combines deep affine and deformable registration. The experimental results showed the efficacy of this method, particularly when used in combination with contour-based methods. The preliminary results look promising. In future work, we plan to extend the approach to a multiframe scheme.

ACKNOWLEDGEMENTS

The work is supported by the Russian Science Foundation grant number 22-21-00125.

REFERENCES

- Avants, B. B., Epstein, C. L., Grossman, M., Gee, J. C., 2008. Symmetric diffeomorphic image registration with cross-correlation: evaluating automated labeling of elderly and neurodegenerative brain. *Medical Image Analysis*, 12(1), 26–41.
- Avants, B. B., Tustison, N., Song, G. et al., 2009. Advanced normalization tools (ANTs). *Insight j*, 2(365), 1–35.
- Balakrishnan, G., Zhao, A., Sabuncu, M. R., Guttag, J., Dalca, A. V., 2019. VoxelMorph: a learning framework for deformable medical image registration. *IEEE Transactions on Medical Imaging*, 38(8), 1788–1800.
- Celikay, K., Chagin, V. O., Cardoso, M. C., Rohr, K., 2022. Denoisereg: Unsupervised joint denoising and registration of time-lapse live cell microscopy images using deep learning. *2022 IEEE 19th International Symposium on Biomedical Imaging (ISBI)*, 1–4.
- De Vos, B. D., Berendsen, F. F., Viergever, M. A., Sokooti, H., Staring, M., Išgum, I., 2019. A deep learning framework for unsupervised affine and deformable image registration. *Medical Image Analysis*, 52, 128–143.
- Gao, Q., Chagin, V. O., Cardoso, M. C., Rohr, K., 2021. Non-rigid registration of live cell nuclei using global optical flow with elasticity constraints. *2021 IEEE 18th International Symposium on Biomedical Imaging (ISBI)*, IEEE, 1457–1460.

- Gao, Q., Rohr, K., 2019. A global method for non-rigid registration of cell nuclei in live cell time-lapse images. *IEEE Transactions on Medical Imaging*, 38(10), 2259–2270.
- Goobic, A. P., Tang, J., Acton, S. T., 2005. Image stabilization and registration for tracking cells in the microvasculature. *IEEE Transactions on Biomedical Engineering*, 52(2), 287–299.
- Jaderberg, M., Simonyan, K., Zisserman, A., Kavukcuoglu, K., 2015. Spatial Transformer Networks. *Proc. of the 28th International Conference on Neural Information Processing Systems*, 2017–2025.
- Kim, I.-H., Chen, Y.-C. M., Spector, D. L., Eils, R., Rohr, K., 2010. Nonrigid registration of 2-D and 3-D dynamic cell nuclei images for improved classification of subcellular particle motion. *IEEE Transactions on Image Processing*, 20(4), 1011–1022.
- Matula, P., Kozubek, M., Dvorák, V., 2006. Fast point-based 3-D alignment of live cells. *IEEE Transactions on Image Processing*, 15(8), 2388–2396.
- Ozere, S., Bouthemy, P., Spindler, F., Paul-Gilloteaux, P., Kervrann, C., 2013. Robust parametric stabilization of moving cells with intensity correction in light microscopy image sequences. *2013 IEEE 10th International Symposium on Biomedical Imaging*, IEEE, 468–471.
- Raza, S.-e.-A., Humayun, A., Abouna, S., Nattkemper, T. W., Epstein, D. B., Khan, M., Rajpoot, N. M., 2012. RAMTaB: robust alignment of multi-tag bioimages. *PLoS One*, 7(2), e30894.
- Ronneberger, O., Fischer, P., Brox, T., 2015. U-net: Convolutional networks for biomedical image segmentation. *Medical Image Computing and Computer-Assisted Intervention—MICCAI 2015: 18th International Conference, Munich, Germany, October 5–9, 2015, Proceedings, Part III 18*, Springer, 234–241.
- Sandkühler, R., Jud, C., Andermatt, S., Cattin, P. C., 2018. AirLab: autograd image registration laboratory. *arXiv preprint arXiv:1806.09907*.
- Sorokin, D. V., Peterlik, I., Tektonidis, M., Rohr, K., Matula, P., 2018. Non-rigid contour-based registration of cell nuclei in 2-D live cell microscopy images using a dynamic elasticity model. *IEEE Transactions on Medical Imaging*, 37(1), 173–184.
- Sorokin, D. V., Suchánková, J., Bártová, E., Matula, P., 2014. Visualizing stable features in live cell nucleus for evaluation of the cell global motion compensation. *Folia biologica*, 60(S1), 45.
- Tektonidis, M., Kim, I.-H., Chen, Y.-C. M., Eils, R., Spector, D. L., Rohr, K., 2015. Non-rigid multi-frame registration of cell nuclei in live cell fluorescence microscopy image data. *Medical Image Analysis*, 19(1), 1–14.
- van de Giessen, M., van der Laan, A., Hendriks, E. A., Vidorreta, M., Reiber, J. H., Jost, C. R., Tanke, H. J., Lelieveldt, B. P., 2011. Fully automated attenuation measurement and motion correction in FLIP image sequences. *IEEE Transactions on Medical Imaging*, 31(2), 461–473.
- Wahba, G., 1990. *Spline models for observational data*. SIAM.
- Wilson, C. A., Theriot, J. A., 2006. A correlation-based approach to calculate rotation and translation of moving cells. *IEEE Transactions on Image Processing*, 15(7), 1939–1951.
- Zhu, W., Huang, Y., Xu, D., Qian, Z., Fan, W., Xie, X., 2021. Test-time training for deformable multi-scale image registration. *2021 IEEE International Conference on Robotics and Automation (ICRA)*, IEEE, 13618–13625.